# Stretchable Graphene Thermistor with Tunable Thermal Index

**Chaoyi Yan, Jiangxin Wang, and Pooi See Lee***

School of Materials Science and Engineering, Nanyang Technological University, 50 Nanyang Avenue, Singapore 639798

**ABSTRACT** Stretchable graphene thermistors with intrinsic high stretchability were fabricated through a lithographic filtration method. Three-dimensional crumpled graphene was used as the thermal detection channels, and silver nanowires were used as electrodes. Both the detection channel and electrodes were fully embedded in an elastomer matrix to achieve excellent stretchability. Detailed temperature sensing properties were characterized at different strains up to 50%. It is evident that the devices can maintain their functionalities even at high stretched states. The devices demonstrated strain-dependent thermal indices, and the sensitivity of the thermistors can be effectively tuned using strain. The unique tunable thermal index is advantageous over conventional rigid ceramic thermistors for diverse and adaptive applications in wearable electronics.

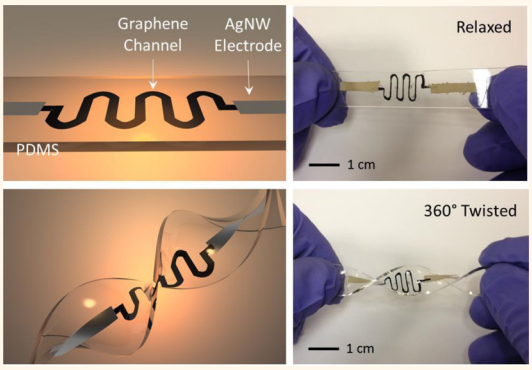


**KEYWORDS:** stretchable electronics · wearable electronics · graphene · thermistor · temperature sensor · embedded elastic conductor

Stretchable electronics represent a type of innovative electronic device which is mechanically soft and conformal and can comply to complex nonplanar surfaces for emerging applications such as wearable electronics.[1] Recent rapid developments of stretchable components and devices such as elastic conductors,[2−7] transistors,[8−11] sensors,[12−16] light-emitting devices,[17−21] and energy sources[22−25] have greatly propagated the fabrication of complex, integrated stretchable systems for practical applications.[26] Temperature sensing is one of the key capabilities of integrated stretchable systems; however, very limited work has been reported to date. Someya *et al.* used organic field-effect transistors mounted on a stretchable mesh for temperature sensing.[27] Buckled Si nanoribbons created by the prestrain strategy[28] were employed as a temperature sensor.[29] Rogers' group demonstrated temperature sensing components in epidermal electronics using serpentine metal (such as platinum[26] or gold[30]) or Si diodes.[30] However, all those works are based on a structural engineering method that limits the device stretchability to 25−30%.[26,27,29,30] Advancements leap-frogging the stretching limit would require alternative strategies such as using intrinsically stretchable materials. Herein we demonstrate the fabrication of stretchable graphene thermistors with high intrinsic stretchability arising from the fully embedded device structure.

Among the several types of temperature sensors, the ceramic-based thermistor is advantageous in terms of fabrication cost, sensitivity, and response speed.[31] Transition metal oxides in bulk or thin film form are the most commonly used materials in thermistors;[32−34] however, the lacking of mechanical flexibility limits their applications in emerging stretchable and wearable devices. Graphene, a one-atom-thick carbon mesh with extraordinary electrical, mechanical, and thermal (high thermal conductivity and strong sensitivity to sample size) properties,[35−38] was recently used in innovative temperature sensors[39,40] as alternatives to conventional rigid ceramics. For example, Kong *et al.* reported the inkjet-printed graphene thermistors on flexible polyethylene terephthalate (PET) substrates for efficient temperature sensing.[40] Note that the strain upon bending is very small (usually below 1%),[41] and most conventional rigid device structures can be readily adopted onto flexible substrates. It is much more challenging to fabricate stretchable

* Address correspondence to pslee@ntu.edu.sg.

Received for review December 29, 2014 and accepted February 6, 2015.

**Published online February 11, 2015**
**10.1021/nn507441c**

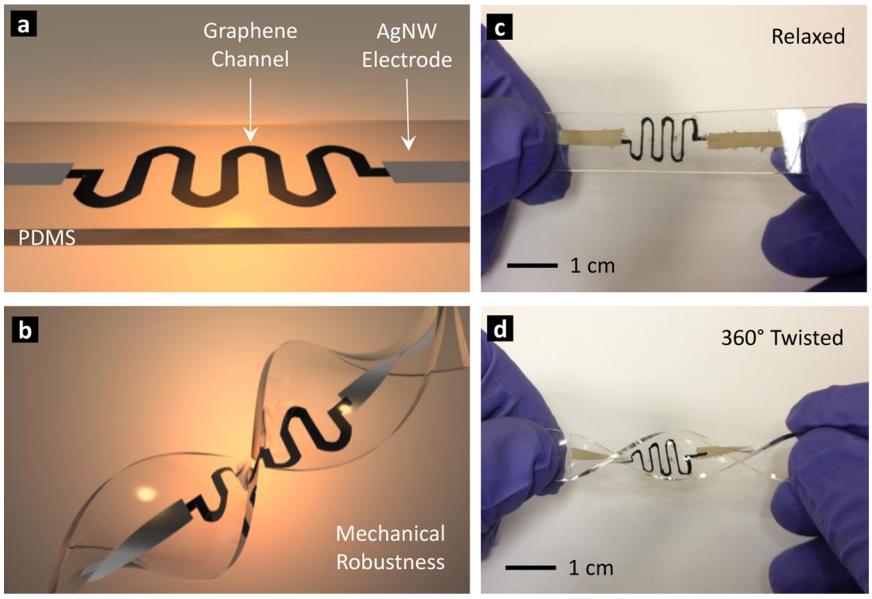


**Figure 1. (a,b) Schematic diagram and (c,d) representative images of the stretchable graphene thermistors at relaxed and twisted states. Highly conductive AgNWs were used as electrodes, and resistive graphene was used as temperature sensing channels. The stretchable devices are mechanically robust and can be deformed into various shapes without fracture.**

devices where the strain is much higher (>30%); that is, the electronic device has to maintain its functionality even when the device is severely mechanically deformed. In this report, graphene thermistors were stretched up to 50% and the corresponding temperature sensing performances were characterized. The devices possess high intrinsic stretchability with fully embedded silver nanowire (AgNW) electrodes and graphene detection channels. Interestingly, we found that the thermal index (an indicator of thermistor sensitivity defined by $B = E_a/2k$, where $B$ is thermal index, $E_a$ is activation energy, and $k$ is Boltzmann constant)[42] of our graphene thermistors can be effectively tuned by mechanical strain. The observed unique property is intrinsic to soft electronics and is in sharp contrast to conventional rigid thermal sensors where the device characteristics cannot be tuned once the device is made. The tunable thermal sensitivity together with the soft nature of our graphene devices paves the way for future diverse and adaptable applications such as temperature sensing, mapping, and compensation in stretchable and wearable electronics.

## RESULTS AND DISCUSSION

Figure 1 shows the schematic diagrams and corresponding images of the stretchable graphene thermistors at relaxed and mechanically deformed states. The devices were fabricated using a lithographic filtration method we developed earlier,[13] which allows facile nanomaterial assembly into desired patterns for different target applications. AgNWs were used as electrodes, and graphene (with nanocellulose binder) was used as the temperature sensing channel. All electrodes and detection channels were fully embedded inside a polydimethylsiloxane (PDMS) matrix (Figure 2d) vto achieve intrinsic high stretchability while maintaining thermal sensing properties (up to 50% strain as demonstrated in this work). The highly conductive AgNWs were selected as stretchable electrodes for easy and consistent electrical measurements. The graphene channel was designed into serpentine shape to augment its resistance within limited space and enhance its dominant role in the thermistor devices. For example, the resistances of AgNW electrodes and the graphene detection channel are compared in Figure S1, Supporting Information. The resistance of AgNWs is ~6 orders of magnitude lower than that of graphene, thus its contribution to the overall device resistance is negligible.

Microstructural characterizations of the graphene thermistors are shown in Figure 2. Figure 2a is the scanning electron microscopy (SEM) image of the AgNW–graphene junction after filtration but before being embedded into the PDMS matrix (see also Figure S2, Supporting Information). The AgNW film lies on the bottom with graphene film covered on top. Enlarged views of the AgNW electrodes and graphene channel are shown in Figure 2b,c, respectively. The assembled AgNW and graphene films exhibited macroporous structures, which are critical for their successful embedding into the PDMS substrate to achieve excellent stretchability. In particular, unlike previous compact graphene paper based on planar graphene nanosheets,[43] the macroporous structure of our graphene detection channel originates from its unique crumpled morphology.[12] Figure 2d is the SEM image of the

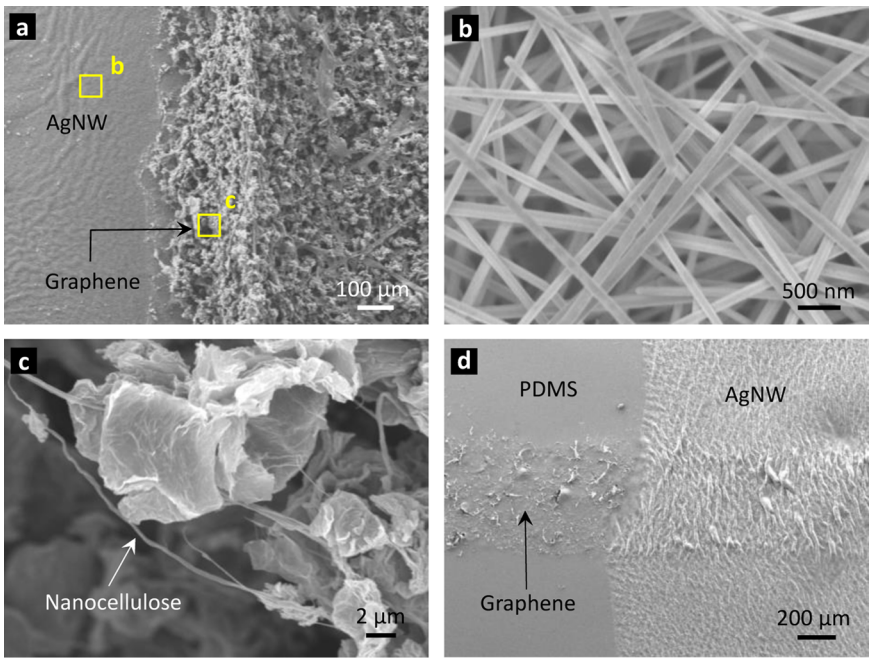


**Figure 2. (a) SEM image of the AgNW−graphene junction before being embedded into PDMS. (b,c) Enlarged views of the AgNW electrode and graphene detection channel. Nanocellulose was used as the binder to improve the processability of crumpled graphene. (d) SEM image of the junction area after being embedded into the PDMS matrix.**

junction area after being embedded into PDMS. Note that the AgNW film which was originally below the graphene channel (Figure 2a) is now exposed on top as the contacting electrodes (see schematic illustration in Figure S2, Supporting Information). It is evident that both AgNW film and graphene channels are fully embedded inside the PDMS substrate, enabling outstanding stretchability and mechanical robustness.

Figure 3a shows the images of the stretchable graphene thermistor at relaxed (0% strain) and stretched (50% strain) states. We first measured the thermistor performance at the relaxed state. Figure 3b shows the $I-V$ curves of the thermistor when temperature was increased from 30 to 100 °C (plotting step is 10 °C for clarity, although the measurement step is 5 °C). At a fixed voltage of 10 V, the current of the device increased from 0.79 $\mu$A at 30 °C to 1.34 $\mu$A at 100 °C, a clear indicator of negative temperature coefficient (NTC) behavior.[31] Figure 3c shows the resistance variation with temperature, which provides a direct view of the decreasing device resistance upon heating. The resistance decreased from 12.63 MΩ at 30 °C to 7.45 MΩ at 100 °C. A closer examination of Figure 3c suggests that the resistance did not vary linearly with temperature (see fitting curves in Figure S3, Supporting Information) but can be described with the following expression:[37]

$$R = R_0 \exp\left(\frac{E_a}{2kT}\right) = R_0 \exp\left(\frac{B}{T}\right) \qquad (1)$$

where $R$ is the resistance at temperature $T$, $R_0$ is the resistance at $T = \infty$, $E_a$ is the thermal activation energy, $k$ is the Boltzmann constant, and $B$ is the thermal index. Equation 1 can be rewritten as

$$\ln(R) = \ln(R_0) + \frac{E_a}{2kT} = \ln(R_0) + \frac{B}{T} \qquad (2)$$

where a linear relationship between ln($R$) and 1/$T$ is expected. The dependence of ln($R$) on 1/$T$ for our graphene thermistor is shown in Figure 3d, where the straight line is the linear fitting result for measured data (open circles). The linear relationship is of great importance for practical applications as it simplifies the post-measurement processing steps.

The graphene thermistor performances at stretched states were characterized in Figure 4. The device was placed on a glass slide substrate, stretched to desired strains, and fixed using binder clips (Figure S4, Supporting Information). Good Ohmic conductions were observed at all strains within 0−50% (Figure S5, Supporting Information). The dependence of thermistor resistance on temperature at different strains is shown in Figure 4a (strain step 10%). It is evident that the graphene thermistor can maintain its functionality even when being stretched up to 50%. The decreasing trends of resistance with temperature indicate consistent NTC behaviors. Fitting curves for ln($R$) *versus* 1/$T$ at different strains are shown in Figure 4b, and excellent linear relationships were observed for all strains, although the fitted slopes (corresponding to thermal index $B$, based on eq 2) changed with strains. While a low index of 847 K was obtained at 0% strain, the index increased to 1203 K at 10% strain. Relatively stable thermal indexes within 1200−1400 K were maintained

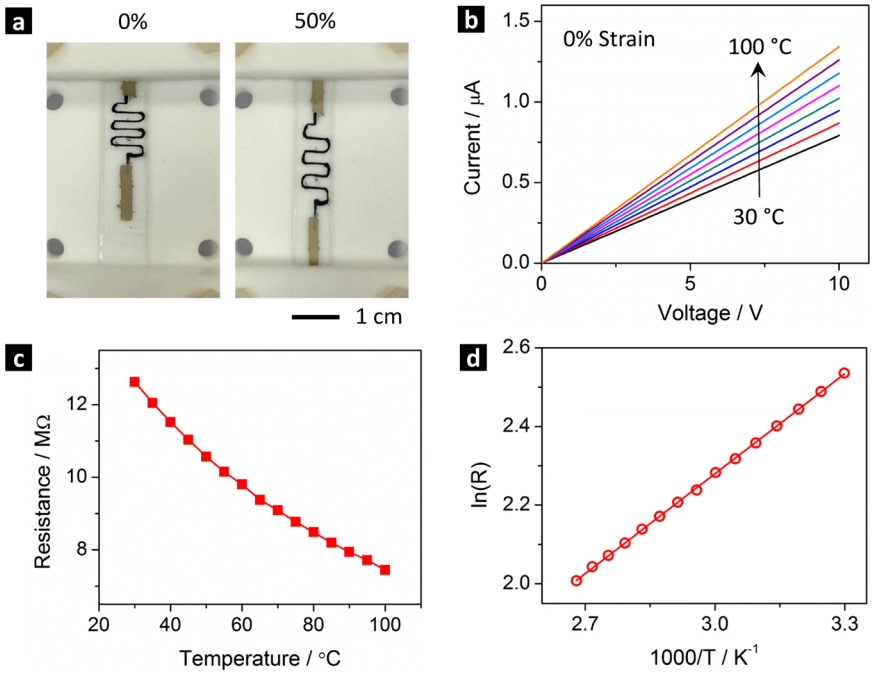


**Figure 3. (a) Images of the stretchable graphene thermistor at 0 and 50% strains. (b) *I*−*V* curves of the thermistor at 0% strain in the temperature range of 30−100 °C (temperature step set as 10 °C for clarity). (c) Resistance variation with temperature showing a nonlinear relationship. (d) Dependence of ln(*R*) on 1000/*T* showing a linear relationship.**

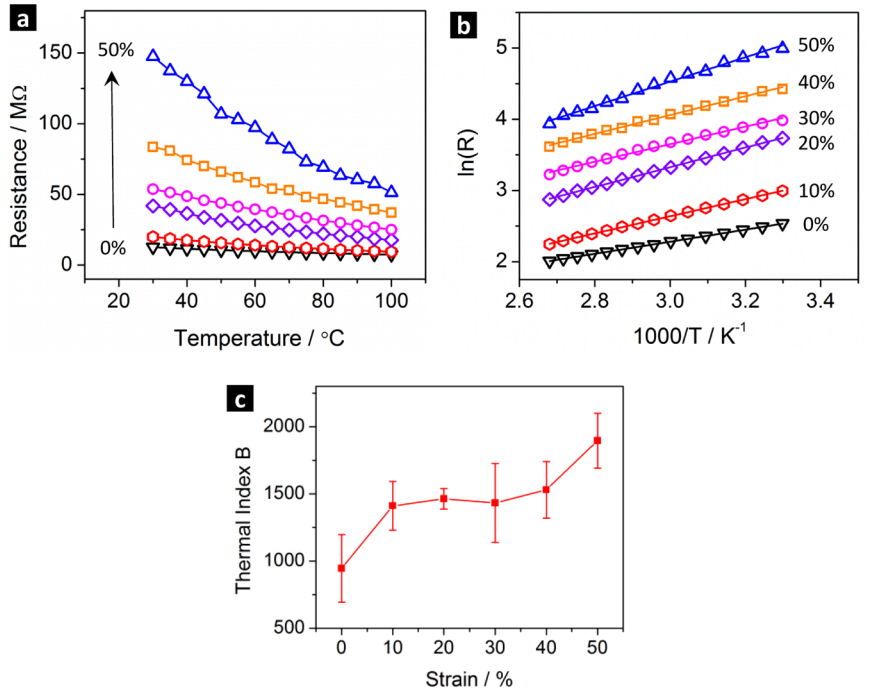


**Figure 4. Graphene thermistor performance variation upon stretching. (a) Resistance variation with temperature (30−100 °C) within 0−50% strains (step 10%). (b) Fitting curves showing the linear dependence of ln(*R*) on 1/*T* at all strains. (c) Thermal index *B* variation with strains (0−50%).**

within 10−40% strains but increased to 1712 K upon further stretching to 50%. Figure 4c shows the thermal index variation upon stretching based on measurements of three devices. An increasing trend of thermal index was observed upon stretching. Note that the thermal sensing properties of graphene thermistors are stable. The thermal index can return to initial values after repeated mechanical stretching to 50% for 100 cycles (Figure S6, Supporting Information).

Other important characteristics of thermistors such as $E_a$ and temperature coefficient of resistance (TCR)

**TABLE 1. Device Performance Variation with Strains within 0−50%**

| strain (%) | thermal index, $B$ (K) | activation energy, $E_a$ (eV) | TCR at 300 K (% $K^{-1}$) |
|---|---|---|---|
| 0 | 945 ± 252 | 0.16 ± 0.04 | −1.05 ± 0.28 |
| 10 | 1411 ± 181 | 0.24 ± 0.03 | −1.57 ± 0.20 |
| 20 | 1463 ± 76 | 0.25 ± 0.01 | −1.63 ± 0.08 |
| 30 | 1432 ± 294 | 0.25 ± 0.05 | −1.59 ± 0.33 |
| 40 | 1530 ± 211 | 0.26 ± 0.04 | −1.70 ± 0.23 |
| 50 | 1895 ± 204 | 0.33 ± 0.04 | −2.11 ± 0.23 |

within 0−50% strains are also calculated, as shown in Table 1. From eq 2, $E_a$ can be obtained using

$$E_a = 2kB \tag{3}$$

TCR is defined by the following expression:[40]

$$\mathrm{TCR} = \frac{dR}{dT} \cdot \frac{1}{R} \tag{4}$$

Combining eqs 2 and 4, we can correlate TCR to thermal index as follows:

$$\mathrm{TCR} = -\frac{B}{T^2} \tag{5}$$

The TCR values for graphene thermistors in Table 1 are calculated at room temperature (300 K) as universally adopted for conventional ceramic devices.[31] The negative signs indicate the NTC behaviors of graphene thermistors.

The temperature-dependent electrical properties of graphene have received significant attention. Due to its unique electrical properties (semi-metal with zero band gap), studies on pristine graphene (mainly fabricated by mechanical exfoliation) have led to quite diverse results, where both increasing[44,45] and decreasing[46] trends of device resistivity at increasing temperature were reported. The resistivity dependence on temperature is a combined effect of semiconducting behavior (dominated by thermally activated charge carriers; resistance decreases at higher temperature) and metallic behavior (dominated by charge carrier scattering; resistance increases at higher temperature). The diverse results originate from the distinct device and measurement conditions, such as graphene crystallinity, layer number, carrier density, scatter wave interference, *etc.*[47] For example, metallic behaviors are usually observed for graphene with high carrier density, which might be induced by gate bias, but semiconducting behavior is usually observed for samples with a Fermi level near the Dirac (charge neutrality) point. However, studies on chemically derived graphene (reduced graphene oxide) suggested quite consistent semiconductor-like behaviors.[39,40] This is because it is very difficult to completely reduce graphene oxide; the remnant oxygen and hydroxyl groups on the surface convert zero-gap graphene into a finite-gap semiconductor or even insulator at high oxygen coverage.[48,49] This is consistent with our observations, where the measured NTC characteristics of our stretchable graphene thermistors are clear indicators of intrinsic semiconducting behaviors. Meanwhile, we suggest that the chemically derived, more defective graphene is beneficial to the thermistor sensitivity. Structural defects such as those derived from chemical processing steps can reduce carrier densities as well as thermal conductivity. A lower carrier density is preferred to achieve higher sensitivity of NTC thermistors. For example, Wang *et al.*[50] reported that the temperature coefficient of resistance of Si nanowire temperature sensors increased from −0.15 to −0.37% $K^{-1}$ when the doping concentration was reduced from $3 \times 10^{16}$ to $4 \times 10^{15}$/cm$^3$. The thermally activated carriers can induce larger resistance variations when the carrier density is low.

Thermal index $B$ is an indicator of thermistor sensitivity. Devices with low $B$ values are useful in circuit temperature compensation and cryogenic measurements, and high $B$ value devices are desired for high-temperature sensing.[31] Most ceramic materials (typically transition metal oxides) exhibit thermal indexes within 2000−5000 K.[31] The thermal indexes of our graphene thermistor are lower than those for conventional ceramic devices but are comparable with previous graphene-based devices. For example, graphene on flexible PET substrates showed a thermal index of 1860 K within the temperature range of 298−358 K.[37] Interestingly, this is the first demonstration of thermistors with tunable thermal index. Conventional rigid thermistors have fixed device structure and hence performance characteristics which cannot be tuned for diverse applications. However, our stretchable graphene thermistors with robust mechanical properties allow facile tuning of electrical resistances and thermal sensitivity, which may open up innovative practical applications. Although the thermistors in this work are yet capable of sensing temperature where the strain also changes (since stretching also induces resistance change), they can find applications like temperature mapping of nonplanar curvilinear surfaces where there is no variations of strains; moreover, the thermal indexes can be effectively tuned for applications at different occasions.

The strain-dependent thermal sensitivity can be understood based on the contact-resistance-dominated electrical conduction, although detailed mechanisms will require further studies. The device resistances are dominated by contact resistances. For example, the resistance (at 30 °C) changed from 12 MΩ at 0% strain to 147 MΩ at 50% strain (Figure 4a). The resistance variation mainly comes from the contact resistance since the crumpled graphene balls are analogous to crumpled conducting paper balls with structures similar to those of buckled structures/surfaces that showed no resistance change with strains.[1,25] Upon stretching, the interconnected crumpled graphene "balls" were

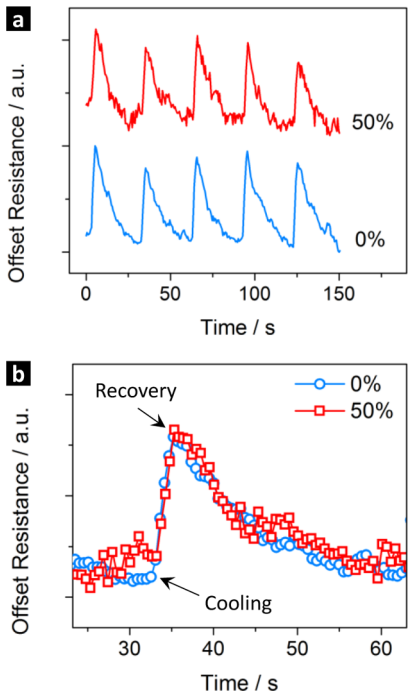


**Figure 5. (a) Response behaviors of the graphene thermistor at 0 and 50% strains. (b) Detailed view and comparison of a single response at 0 and 50% strains, showing the similar response behaviors at different strains.**

stretched, resulting in decreased contact areas and hence increased contact resistances, which is equivalent to the increase of conduction barrier height. That is, charge carriers have to overcome higher conduction barriers at stretched states. Analogous conduction-barrier-dominated resistance was also observed in previous percolating semiconductor nanowire films.[51] The conduction barrier at the semiconductor–semiconductor interface is composed of two back-to-back surface depletion layers, and the width of the depletion layer $W$ can be described using[52]

$$W \propto \sqrt{\frac{V}{N}} \qquad (6)$$

where $V$ is the barrier height and $N$ is the carrier density. Thus, for a certain increase of charge carrier density (thermally activated), a larger decrease of depletion layer width is expected for higher barriers based on eq 6. This may help to explain the fact that our graphene thermistors exhibited a trend of higher sensitivity at stretched states due to the more significant conduction barrier modulations at higher strain.

Response behaviors of the graphene thermistors are shown in Figure 5. The device was held at 50 °C with intentionally introduced temperature perturbations for response measurements. To prevent the effect of strain-induced resistance change, a touchless temperature perturbation was employed by blowing cool air (room temperature, 25 °C) to the hot device surface. A typical cooling perturbation period was 3 s, after which the device was allowed to recover to its background temperature (50 °C) naturally. Response behaviors at 0 and 50% strains are shown in Figure 5a. Detailed views of a single response cycle from 0 and 50% strains are compared in Figure 5b. The resistance increased rapidly upon cooling and then gradually recovered when the cooling perturbation was stopped. Similar response and recovery behaviors were observed at 0 and 50% strains (Figure 5b). The thermal responses of graphene thermistors were dominated by the heat transfer processes. Since the graphene detection channel was exposed on top of the PDMS matrix (Figure S7, Supporting Information), cool air was in direct contact with the graphene channel and a fast response process was observed. The recovery process (~20 s, Figure 5b) was slower than the response process because the recovery was determined by the rate of heat transfer from the underlying heating stage, through the glass slide and PDMS substrates to the graphene detection channel. PDMS has a low thermal conductivity of 0.15 $W \cdot m^{-1} \cdot K^{-1}$ (at 25 °C),[53] and for comparison, glass substrates (soda lime microscope glass) typically exhibit thermal conductivity of 0.9–1.3 $W \cdot m^{-1} \cdot K^{-1}$ (at 25 °C),[54] which is at least 6 times as high as that for PDMS. Thus, the thermal conduction through the PDMS substrate is the rate-limiting step for the recovery process. Note that the PDMS substrate and hence embedded graphene layer may undergo slight relaxation during the response measurements at 50% strain. The relaxation may induce contact instability between the crumpled graphene balls and lead to larger noise on the measurements, as observed in Figure 5. It is evident that our graphene thermistors can respond and recover very fast within tens of seconds, which is beneficial for their practical applications such as wearable temperature sensing. The response speed can be further optimized. For example, the substrate thickness can be reduced to expedite the heat transfer process; a thinner substrate with lower thermal capacity will lead to faster heating or cooling rates. Alternative stretchable substrates with higher thermal conductivity are also desired to improve the response speeds.

## CONCLUSIONS

In conclusion, we demonstrate the fabrication and characterizations of highly stretchable graphene thermistors based on conductive AgNW electrodes and a resistive graphene detection channel. Typical semiconductor-like NCT behaviors were observed. The devices were stretched up to 50% and could maintain their functionality even at highly stretched states. Linear relationships between ln($R$) and 1/$T$ were observed at all strains within 0–50%, indicating consistent device characteristics. An increasing trend of thermal index $B$ upon stretching was observed, which was attributed to the strain-induced electrical connection change

between adjacent crumpled graphene. The tunable thermal index is a unique feature of soft electronics as compared with conventional ceramic thermal sensors with unchangeable device characteristics and is expected to enable diverse applications for the same graphene thermistor. Response behavior measurements revealed fast response speeds of the stretchable thermistors at both relaxed and stretched states. Fast response and recovery within tens of seconds were achieved. The innovative stretchable graphene thermistor holds great promise for future wearable temperature sensing applications.

## METHODS

**Device Fabrication.** The stretchable graphene thermistors were fabricated using our innovative lithographic filtration methods as described earlier.[12] Briefly, crumpled graphene (Time Nano, China) was fabricated by thermal reduction at 1200 °C with inert $N_2$ atmosphere. The unique crumpled morphology was attributed to the capillary force as has also been observed during graphene ball formation.[55] Nanocellulose fibril (University of Maine, USA) was used as the binder to improve the processability of crumpled graphene. For device fabrication, AgNWs (diameter 40−100 nm, length 20−100 $\mu$m, Seashell Technology LLC, USA) dispersed in ethanol (1 mg mL$^{-1}$) were first filtered as electrodes using polycarbonate (PC) filter membranes (Millipore GTTP, pore size 220 nm). Graphene and nanocellulose dispersed in deionized water (1 mg mL$^{-1}$, weight ratio 1:1) were then filtered as the detection channel to connect the AgNW electrodes. Filtration masks with straight (for AgNW filtration) and serpentine (for graphene/nanocellulose filtration) patterns were used to obtain nanomaterial films with desired patterns. The PDMS base and curer (Sylgard 184, Dow Corning, USA) in liquid form was thoroughly mixed, poured on top of the filtered AgNW and graphene films, degassed in a vacuum desiccator for 30 min, and then cured at 60 °C for 2 h. The functional AgNW electrodes and graphene detection channels were fully embedded inside the PDMS matrix, and highly stretchable devices were obtained after peeling off the solidified PDMS from the PC filter membrane.

**Device Characterization and Testing.** The devices were characterized using field-emission SEM (JSM 7600F, Japan). Electrical properties of the thermistors were measured using a Keithley analyzer (model 4200) equipped with a heating stage. For measurements at stretched states, the device was placed on a glass slide substrate, stretched to desired strains, and then fixed at the two ends using binder clips. The temperature was increased from 30 to 100 °C with a step of 5 °C. The device was stabilized for 5 min to achieve thermal equilibrium at each temperature point before electrical measurements. A stainless steel block was placed under the glass slide substrate for heat transfer between the heating stage and thermistor device. Home-built stretching stages were also used to show the excellent stretchability of the graphene thermistors.

*Conflict of Interest:* The authors declare no competing financial interest.

*Supporting Information Available:* AgNW and graphene resistance comparison, schematics of device structure, and *I*−*V* curves at different strains. This material is available free of charge *via* the Internet at http://pubs.acs.org.

*Acknowledgment.* This work was supported in part by the Singapore National Research Foundation (CREATE Programme of Nanomaterials for Energy and Water Management). The authors thank X.W. Lu and X.W. Yan for their technical support and insightful discussions.

## REFERENCES AND NOTES

1. Rogers, J. A.; Someya, T.; Huang, Y. G. Materials and Mechanics for Stretchable Electronics. *Science* **2010**, *327*, 1603.
2. Xu, F.; Zhu, Y. Highly Conductive and Stretchable Silver Nanowire Conductors. *Adv. Mater.* **2012**, *24*, 5117.
3. Yun, S.; Niu, X. F.; Yu, Z. B.; Hu, W. L.; Brochu, P.; Pei, Q. B. Compliant Silver Nanowire−Polymer Composite Electrodes for Bistable Large Strain Actuation. *Adv. Mater.* **2012**, *24*, 1321.
4. Lee, P.; Lee, J.; Lee, H.; Yeo, J.; Hong, S.; Nam, K. H.; Lee, D.; Lee, S. S.; Ko, S. H. Highly Stretchable and Highly Conductive Metal Electrode by Very Long Metal Nanowire Percolation Network. *Adv. Mater.* **2012**, *24*, 3326.
5. Moon, G. D.; Lim, G.-H.; Song, J. H.; Shin, M.; Yu, T.; Lim, B.; Jeong, U. Highly Stretchable Patterned Gold Electrodes Made of Au Nanosheets. *Adv. Mater.* **2013**, *25*, 2707.
6. Zhu, Y.; Xu, F. Buckling of Aligned Carbon Nanotubes as Stretchable Conductors: A New Manufacturing Strategy. *Adv. Mater.* **2012**, *24*, 1073.
7. Lacour, S. P.; Wagner, S.; Huang, Z.; Suo, Z. Stretchable Gold Conductors on Elastomeric Substrates. *Appl. Phys. Lett.* **2003**, *82*, 2404.
8. Xu, F.; Wu, M.-Y.; Safron, N. S.; Roy, S. S.; Jacobberger, R. M.; Bindl, D. J.; Seo, J.-H.; Chang, T.-H.; Ma, Z.; Arnold, M. S. Highly Stretchable Carbon Nanotube Transistors with Ion Gel Gate Dielectrics. *Nano Lett.* **2014**, *14*, 682.
9. Chae, S. H.; Yu, W. J.; Bae, J. J.; Duong, D. L.; Perello, D.; Jeong, H. Y.; Ta, Q. H.; Ly, T. H.; Vu, Q. A.; Yun, M.; et al. Transferred Wrinkled $Al_2O_3$ for Highly Stretchable and Transparent Graphene−Carbon Nanotube Transistors. *Nat. Mater.* **2013**, *12*, 403.
10. Chortos, A.; Lim, J.; To, J. W. F.; Vosgueritchian, M.; Dusseault, T. J.; Kim, T.-H.; Hwang, S.; Bao, Z. Highly Stretchable Transistors Using a Microcracked Organic Semiconductor. *Adv. Mater.* **2014**, *26*, 4253.
11. Lee, S.-K.; Kim, B. J.; Jang, H.; Yoon, S. C.; Lee, C.; Hong, B. H.; Rogers, J. A.; Cho, J. H.; Ahn, J.-H. Stretchable Graphene Transistors with Printed Dielectrics and Gate Electrodes. *Nano Lett.* **2011**, *11*, 4642.
12. Yan, C.; Wang, J.; Kang, W.; Cui, M.; Wang, X.; Foo, C. Y.; Chee, K. J.; Lee, P. S. Highly Stretchable Piezoresistive Graphene−Nanocellulose Nanopaper for Strain Sensors. *Adv. Mater.* **2014**, *26*, 2022.
13. Yan, C.; Wang, J.; Wang, X.; Kang, W.; Cui, M.; Foo, C. Y.; Lee, P. S. An Intrinsically Stretchable Nanowire Photodetector with a Fully Embedded Structure. *Adv. Mater.* **2014**, *26*, 943.
14. Ko, H. C.; Stoykovich, M. P.; Song, J. Z.; Malyarchuk, V.; Choi, W. M.; Yu, C. J.; Geddes, J. B.; Xiao, J. L.; Wang, S. D.; Huang, Y. G.; et al. A Hemispherical Electronic Eye Camera Based on Compressible Silicon Optoelectronics. *Nature* **2008**, *454*, 748.
15. Song, Y. M.; Xie, Y.; Malyarchuk, V.; Xiao, J.; Jung, I.; Choi, K.-J.; Liu, Z.; Park, H.; Lu, C.; Kim, R.-H.; et al. Digital Cameras with Designs Inspired by the Arthropod Eye. *Nature* **2013**, *497*, 95.
16. Lipomi, D. J.; Vosgueritchian, M.; Tee, B. C. K.; Hellstrom, S. L.; Lee, J. A.; Fox, C. H.; Bao, Z. N. Skin-like Pressure and Strain Sensors Based on Transparent Elastic Films of Carbon Nanotubes. *Nat. Nanotechnol.* **2011**, *6*, 788.
17. Filiatrault, H. L.; Porteous, G. C.; Carmichael, R. S.; Davidson, G. J. E.; Carmichael, T. B. Stretchable Light-Emitting Electrochemical Cells Using an Elastomeric Emissive Material. *Adv. Mater.* **2012**, *24*, 2673.
18. Yu, Z. B.; Niu, X. F.; Liu, Z. T.; Pei, Q. B. Intrinsically Stretchable Polymer Light-Emitting Devices Using Carbon Nanotube−Polymer Composite Electrodes. *Adv. Mater.* **2011**, *23*, 3989.

19. Sekitani, T.; Nakajima, H.; Maeda, H.; Fukushima, T.; Aida, T.; Hata, K.; Someya, T. Stretchable Active-Matrix Organic Light-Emitting Diode Display Using Printable Elastic Conductors. *Nat. Mater.* **2009**, *8*, 494.
20. Liang, J.; Li, L.; Niu, X.; Yu, Z.; Pei, Q. Elastomeric Polymer Light-Emitting Devices and Displays. *Nat. Photonics* **2013**, *7*, 817.
21. White, M. S.; Kaltenbrunner, M.; Glowacki, E. D.; Gutnichenko, K.; Kettlgruber, G.; Graz, I.; Aazou, S.; Ulbricht, C.; Egbe, D. A. M.; Miron, M. C.; et al. Ultrathin, Highly Flexible and Stretchable PLEDs. *Nat. Photonics* **2013**, *7*, 811.
22. An, K. H.; Kim, W. S.; Park, Y. S.; Choi, Y. C.; Lee, S. M.; Chung, D. C.; Bae, D. J.; Lim, S. C.; Lee, Y. H. Supercapacitors Using Single-Walled Carbon Nanotube Electrodes. *Adv. Mater.* **2001**, *13*, 497.
23. Gaikwad, A. M.; Zamarayeva, A. M.; Rousseau, J.; Chu, H. W.; Derin, I.; Steingart, D. A. Highly Stretchable Alkaline Batteries Based on an Embedded Conductive Fabric. *Adv. Mater.* **2012**, *24*, 5071.
24. Lee, J.; Wu, J. A.; Shi, M. X.; Yoon, J.; Park, S. I.; Li, M.; Liu, Z. J.; Huang, Y. G.; Rogers, J. A. Stretchable GaAs Photovoltaics with Designs That Enable High Areal Coverage. *Adv. Mater.* **2011**, *23*, 986.
25. Lipomi, D. J.; Tee, B. C. K.; Vosgueritchian, M.; Bao, Z. N. Stretchable Organic Solar Cells. *Adv. Mater.* **2011**, *23*, 1771.
26. Kim, D. H.; Lu, N. S.; Ma, R.; Kim, Y. S.; Kim, R. H.; Wang, S. D.; Wu, J.; Won, S. M.; Tao, H.; Islam, A.; et al. Epidermal Electronics. *Science* **2011**, *333*, 838.
27. Someya, T.; Kato, Y.; Sekitani, T.; Iba, S.; Noguchi, Y.; Murase, Y.; Kawaguchi, H.; Sakurai, T. Conformable, Flexible, Large-Area Networks of Pressure and Thermal Sensors with Organic Transistor Active Matrixes. *Proc. Natl. Acad. Sci. U.S.A.* **2005**, *102*, 12321.
28. Khang, D. Y.; Jiang, H. Q.; Huang, Y.; Rogers, J. A. A Stretchable Form of Single-Crystal Silicon for High-Performance Electronics on Rubber Substrates. *Science* **2006**, *311*, 208.
29. Yu, C.; Wang, Z.; Yu, H.; Jiang, H. A Stretchable Temperature Sensor Based on Elastically Buckled Thin Film Devices on Elastomeric Substrates. *Appl. Phys. Lett.* **2009**, *95*, 141912.
30. Webb, R. C.; Bonifas, A. P.; Behnaz, A.; Zhang, Y.; Yu, K. J.; Cheng, H.; Shi, M.; Bian, Z.; Liu, Z.; Kim, Y.-S.; et al. Ultrathin Conformal Devices for Precise and Continuous Thermal Characterization of Human Skin. *Nat. Mater.* **2013**, *12*, 938.
31. Feteira, A. Negative Temperature Coefficient Resistance (NTCR) Ceramic Thermistors: An Industrial Perspective. *J. Am. Ceram. Soc.* **2009**, *92*, 967.
32. Feltz, A.; Polzl, W. Spinel Forming Ceramics of the System $Fe_xNi_yMn_{3-x-y}O_4$ for High Temperature NTC Thermistor Applications. *J. Eur. Ceram. Soc.* **2000**, *20*, 2353.
33. Nobre, M. A. L.; Lanfredi, S. Grain Boundary Electric Characterization of $Zn_7Sb_2O_{12}$ Semiconducting Ceramic: A Negative Temperature Coefficient Thermistor. *J. Appl. Phys.* **2003**, *93*, 5576.
34. Park, K.; Bang, D. Y. Electrical Properties of Ni-Mn-Co-(Fe) Oxide Thick-Film NTC Thermistors Prepared by Screen Printing. *J. Mater. Sci.* **2003**, *14*, 81.
35. Geim, A. K.; Novoselov, K. S. The Rise of Graphene. *Nat. Mater.* **2007**, *6*, 183.
36. Balandin, A. A. Thermal Properties of Graphene and Nanostructured Carbon Materials. *Nat. Mater.* **2011**, *10*, 569.
37. Shahil, K. M. F.; Balandin, A. A. Thermal Properties of Graphene and Multilayer Graphene: Applications in Thermal Interface Materials. *Solid State Commun.* **2012**, *152*, 1331.
38. Renteria, J.; Nika, D.; Balandin, A. Graphene Thermal Properties: Applications in Thermal Management and Energy Storage. *Appl. Sci.* **2014**, *4*, 525.
39. Al-Mumen, H.; Fubo, R.; Lixin, D.; Wen, L. Design, Fabrication, and Characterization of Graphene Thermistor. *8th IEEE International Conference on Nano/Micro Engineered and Molecular Systems (NEMS)*, April 7–10, 2013; p 1135.
40. Kong, D.; Le, L. T.; Li, Y.; Zunino, J. L.; Lee, W. Temperature-Dependent Electrical Properties of Graphene Inkjet-Printed on Flexible Materials. *Langmuir* **2012**, *28*, 13467.
41. Yu, T.; Ni, Z.; Du, C.; You, Y.; Wang, Y.; Shen, Z. Raman Mapping Investigation of Graphene on Transparent Flexible Substrate: The Strain Effect. *J. Phys. Chem. C* **2008**, *112*, 12602.
42. Cao, J. L.; Wang, Z. X.; Zhan, X. Y.; Wang, Q. S.; Safdar, M.; Wang, Y. J.; He, J. Vertical SnSe Nanorod Arrays: from Controlled Synthesis and Growth Mechanism to Thermistor and Photoresistor. *Nanotechnology* **2014**, *25*, 105705.
43. Sumboja, A.; Foo, C. Y.; Wang, X.; Lee, P. S. Large Areal Mass, Flexible and Free-Standing Reduced Graphene Oxide/Manganese Dioxide Paper for Asymmetric Supercapacitor Device. *Adv. Mater.* **2013**, *25*, 2809.
44. Morozov, S. V.; Novoselov, K. S.; Katsnelson, M. I.; Schedin, F.; Elias, D. C.; Jaszczak, J. A.; Geim, A. K. Giant Intrinsic Carrier Mobilities in Graphene and Its Bilayer. *Phys. Rev. Lett.* **2008**, *100*, 016602.
45. Bolotin, K. I.; Sikes, K. J.; Hone, J.; Stormer, H. L.; Kim, P. Temperature-Dependent Transport in Suspended Graphene. *Phys. Rev. Lett.* **2008**, *101*, 096802.
46. Shao, Q.; Liu, G.; Teweldebrhan, D.; Balandin, A. A. High-Temperature Quenching of Electrical Resistance in Graphene Interconnects. *Appl. Phys. Lett.* **2008**, *92*, 202108.
47. Skákalová, V.; Kaiser, A. B.; Yoo, J. S.; Obergfell, D.; Roth, S. Correlation between Resistance Fluctuations and Temperature Dependence of Conductivity in Graphene. *Phys. Rev. B* **2009**, *80*, 153404.
48. Ito, J.; Nakamura, J.; Natori, A. Semiconducting Nature of the Oxygen-Adsorbed Graphene Sheet. *J. Appl. Phys.* **2008**, *103*, 113712.
49. Boukhvalov, D. W.; Katsnelson, M. I. Modeling of Graphite Oxide. *J. Am. Chem. Soc.* **2008**, *130*, 10697.
50. Wang, C.-P.; Liu, C.-W.; Gau, C. Silicon Nanowire Temperature Sensor and Its Characteristic. *IEEE International Conference on Nano/Micro Engineered and Molecular Systems (NEMS)*, February 20–23, 2011; p 630.
51. Yan, C.; Singh, N.; Lee, P. S. Wide-Bandgap $Zn_2GeO_4$ Nanowire Networks as Efficient Ultraviolet Photodetectors with Fast Response and Recovery Time. *Appl. Phys. Lett.* **2010**, *96*, 053108.
52. Vanheusden, K.; Seager, C. H.; Warren, W. L.; Tallant, D. R.; Voigt, J. A. Correlation between Photoluminescence and Oxygen Vacancies in ZnO Phosphors. *Appl. Phys. Lett.* **1996**, *68*, 403.
53. Mark, J. E. *Polymer Data Handbook*; Oxford University Press: New York, 1999.
54. Janssen, L. P. B. M.; Warmoeskerken, M. M. C. G. *Transport Phenomena Data Companion*; VSSD: Delft, The Netherlands, 2006.
55. Luo, J.; Jang, H. D.; Sun, T.; Xiao, L.; He, Z.; Katsoulidis, A. P.; Kanatzidis, M. G.; Gibson, J. M.; Huang, J. Compression and Aggregation-Resistant Particles of Crumpled Soft Sheets. *ACS Nano* **2011**, *5*, 8943.